A&A, 710, A195 (2026)
https://doi.org/10.1051/0004-6361/202659197
© The Authors 2026

Astronomy & Astrophysics

Magnetoacoustic waves in two-fluid weakly ionised solar atmospheric plasmas in ionisation non-equilibrium

J. Alshehri[1,2,⋆], I. Ballai[1], A. H. Alharbi[3,⋆], G. Verth[1], and V. Fedun[4]

[1] Plasma Dynamics Group, School of Mathematical and Physical Sciences, The University of Sheffield, Hicks Building, Hounsfield Road, Sheffield S3 7RH, United Kingdom
[2] Applied College – Al-Quwaiiyah, Shaqra University, Al-Quwaiiyah 19257, Saudi Arabia
[3] Mathematics Department, Faculty of Sciences, Umm Al-Qura University, Makkah 21955, Saudi Arabia
[4] Plasma Dynamics Group, School of Electrical and Electronic Engineering, The University of Sheffield, Mappin Street, Sheffield S1 3JD, United Kingdom

Received 29 January 2026 / Accepted 25 April 2026

ABSTRACT

Context. In the lower solar atmosphere, the plasma is only weakly ionised, so wave dynamics are governed not only by magnetic forces but also by ion–neutral interactions and chemical processes.
Aims. This paper investigates how ionisation and recombination influence the propagation and damping of magnetoacoustic waves in weakly ionised solar plasmas, and how these effects depend on the strength of collisional coupling, the direction of propagation, and the plasma-β parameter.
Methods. We used a two-fluid model in which charges and neutrals are treated as separate but interacting fluids coupled through collisions, thermal exchange, and ionisation and recombination processes. We analysed linear wave properties by solving the resulting dispersion relation and investigating the angular dependence of the complex wave frequency using Friedrichs diagrams.
Results. Our results confirm that ionisation non-equilibrium introduces an additional relaxation mechanism that can substantially modify wave damping and anisotropy. In weakly collisional regimes, chemical coupling allows neutral slow modes to inherit magnetic anisotropy even when friction is weak. In strongly collisional regimes, neutral slow modes become strongly damped and can transition into non-oscillatory, over-damped behaviour, despite the plasma being weakly ionised. The influence of non-equilibrium effects depends critically on plasma-β. Slow modes are most affected at low β, while at high β the fast mode becomes increasingly compressive and more susceptible to chemical damping. Our results demonstrate that ionisation non-equilibrium plays a key role in determining the nature of wave propagation and dissipation in weakly ionised solar plasmas.

Key words. waves – Sun: chromosphere – Sun: photosphere

1. Introduction

Magnetoacoustic waves are among the most commonly observed wave modes in the solar atmosphere, and they are considered key candidates for the transport and dissipation of the energy that can contribute to chromospheric and coronal heating. However, much of the solar atmosphere, particularly regions like the chromosphere, spicules, and prominences, is only partially ionised, consisting of ions, electrons, and a significant fraction of neutral atoms (Vernazza et al. 1981; Avrett & Loeser 2008; Leenaarts et al. 2011). In these environments, the single-fluid magnetohydrodynamic (MHD) approximation becomes inadequate, necessitating more realistic descriptions that can account for the decoupling between charged and neutral components.

Two-fluid models, which treat the ion-electron plasma and the neutral fluid as interacting but distinct components, provide a more physically accurate framework for investigating wave dynamics in partially ionised media at frequency ranges that are comparable with the collisional frequency of particles (Khomenko et al. 2014). These models capture critical effects such as ion–neutral collisions, drift velocities, and ambipolar diffusion, all of which can significantly alter the propagation and damping characteristics of magnetoacoustic waves (Soler et al. 2013; Martínez-Gómez et al. 2017). Collisions between ions and neutrals introduce strong damping mechanisms that can lead to the rapid attenuation of wave energy – an effect especially pronounced for high-frequency or short-wavelength waves (Zaqarashvili et al. 2011; Ballester et al. 2018; Niedziela et al. 2024; Martínez-Gómez 2025).

Theoretical studies based on two-fluid descriptions have shown that the presence of neutrals can lead to the splitting of wave modes, the modification of dispersion relations, and, in some cases, the appearance of new wave branches not found in fully ionised plasmas. Understanding these effects is essential for interpreting observational data from instruments such as the Interface Region Imaging Spectrograph (IRIS) and Hinode, which have detected signatures of compressible waves across a range of atmospheric heights (De Pontieu et al. 2007; Okamoto & De Pontieu 2011). Moreover, the role of partial ionisation in modulating the energy flux carried by magnetoacoustic waves has direct implications for models of chromospheric heating (Arber et al. 2016; Snow & Hillier 2021; McMurdo et al. 2023, 2025; Kumar et al. 2024).

Previous two-fluid studies have established much of the theoretical framework for magnetoacoustic wave propagation in partially ionised solar plasmas under the assumption of ionisation equilibrium. Using a two-fluid approach, Zaqarashvili et al. (2011) derived the general dispersion relations for MHD waves in a uniform, partially ionised medium and demonstrated that the validity of the single-fluid MHD description is limited to

⋆ Corresponding authors: jhalshehri1@sheffield.ac.uk; ahhrbe@uqu.edu.sa

Open Access article, published by EDP Sciences, under the terms of the Creative Commons Attribution License (https://creativecommons.org/licenses/by/4.0), which permits unrestricted use, distribution, and reproduction in any medium, provided the original work is properly cited.
This article is published in open access under the Subscribe to Open model. Subscribe to A&A to support open access publication.

low-frequency perturbations. Their analysis showed that ion–neutral collisions introduce strong damping at frequencies comparable to the collision frequency and lead to the appearance of additional wave branches associated with the neutral component, particularly for compressive modes. Subsequently, Soler et al. (2013) and Popescu Braileanu et al. (2019) performed detailed parametric studies of magnetoacoustic waves in a two-fluid plasma, examining the influence of the ionisation degree, collision frequency, and plasma-β on wave propagation and attenuation. They identified propagation cutoffs for slow modes, quantified the anisotropic damping of fast and slow magnetoacoustic waves, and derived analytic approximations in the strong-coupling limit that clarify the transition between two-fluid and single-fluid behaviour. While these studies provide a comprehensive description of wave dynamics in ionisation equilibrium, they neglect the effects of time-dependent ionisation and recombination. In contrast, the present work extends the two-fluid framework by incorporating ionisation non-equilibrium processes, allowing us to assess how chemical relaxation modifies the dispersion properties, damping rates, and angular dependence of magnetoacoustic modes. This additional degree of freedom introduces new damping channels that significantly affect slow and neutral modes and lead to qualitative differences in the structure of Friedrichs diagrams that cannot be captured within equilibrium models.

Ionisation and recombination effects have also been incorporated in multi-fluid studies of partially ionised solar plasmas. Leake et al. (2012) and Brchnelova et al. (2023) demonstrated, through time-dependent multi-fluid simulations of chromospheric magnetic reconnection, that ionisation non-equilibrium strongly affects momentum coupling, heating, and energy dissipation in weakly ionised plasmas. Similarly, using a reactive multi-fluid model, Maneva et al. (2017) and Ballai (2019) investigated magnetosonic wave propagation in the chromosphere and showed that impact ionisation and radiative recombination can significantly enhance the damping of compressive waves, providing an additional dissipation mechanism beyond ion–neutral collisions. While these studies highlight the importance of reactive plasma processes in dynamic chromospheric environments, they do not address in detail how ionisation and recombination modify the linear wave spectrum itself. The present work complements these efforts by analysing magnetoacoustic wave propagation and damping in a two-fluid plasma with ionisation non-equilibrium, enabling a direct comparison with equilibrium models and an assessment of the role of chemical relaxation.

In this work, we adopted a two-fluid MHD approach to study the behaviour of magnetoacoustic waves in partially ionised solar plasmas. We analysed how key parameters (such as the ionisation fraction, collision frequency, and magnetic field strength) influence wave propagation, mode coupling, and damping. We aim to provide new insights into the role of ion–neutral interactions in wave energy dissipation and to contribute to the broader understanding of energy transport in the lower solar atmosphere. Although our analysis is not intended to represent a single atmospheric layer, the chosen parameter values were selected to sample weakly ionised regimes that are consistent with semi-empirical models of the lower solar atmosphere, such as the VAL-C model (Vernazza et al. 1981).

2. Physical model and governing equations

In the lower solar atmosphere, the plasma is only weakly ionised, with neutrals constituting the dominant mass component and the ionisation fraction remaining small. Under these conditions, the thermodynamic state of the plasma is largely regulated by ionisation and recombination processes rather than by ion-ion interactions typical of fully ionised plasmas.

In such weakly ionised plasmas, the dominant physical processes governing wave dynamics are elastic collisions, thermal energy exchange, and chemical conversion between charged and neutral particles. Elastic ion–neutral collisions efficiently couple the velocities of the fluids, while collisional heat exchange acts to reduce interspecies temperature differences. Ionisation and recombination introduce additional sinks and sources in the mass, momentum, and energy equations, modifying the effective inertia and thermodynamic response of the plasma. Because recombination continuously removes charged particles, the magnetic influence on the bulk plasma is reduced, and magnetoacoustic waves supported by the ion–electron fluid can experience significant damping through collisional and thermal coupling to neutrals. The resulting wave behaviour reflects a balance between magnetic forces acting on a minority charged component and non-magnetic processes that dominate the energetics of the system.

Recombination and ionisation are crucial processes in solar plasma physics, influencing the evolution and behaviour of plasmas. We assumed a pure hydrogen plasma and the hydrogen atoms with one single energy level (bound level). For simplicity, we assumed that the ionisation degree of the plasma is affected by collisional ionisation and radiative recombination. Ionisation occurs at the collisional encounter of a neutral atom and an electron, and the rate of ionisation is denoted by K_I. Recombination is the result of a collisional interaction of an electron and an ion, and the rate of recombination is denoted by K_R. The plasma is assumed to be thin to ionising radiation, so that every ionising photon emitted during the recombination process can escape.

At this stage, we ought to make two remarks regarding the ionisation and recombination rates used in the literature. Currently, these rates are not unique, but their predicted values are fairly similar. On one hand, Cox & Tucker (1969) and Moore & Fung (1972) give ionisation and recombination rates of

$$\begin{aligned} K_I &= 2.34\times10^{-14}x^{-1/2}e^{-x} \quad (\mathrm{m^3 s^{-1}}),\\ K_R &= 5.2\times10^{-20}x^{1/2}\left(0.4288+\frac{1}{2}\ln x+0.4698x^{-1/3}\right) \ \mathrm{m^3 s^{-1}}), \end{aligned} \tag{1}$$

where $x = \Phi/k_B T$, with $\Phi = 13.6$ eV is the ionisation potential of the hydrogen atom with an electron in the bound state, T is the electron temperature, and $k_B = 8.6\times10^{-5}$ eV K^{-1} is the Boltzmann constant. On the other hand, Voronov (1997) and Smirnov (2003) give these rates as

$$\begin{aligned} K_I &= \frac{A}{C_2+x}x^{C_1}e^{-x} \quad (\mathrm{m^3 s^{-1}}),\\ K_R &= 1.5\times10^{-19}\frac{1}{\sqrt{k_B T}} \quad (\mathrm{m^3 s^{-1}}), \end{aligned} \tag{2}$$

where the constants $A = 2.91\times10^{-14}$, $C_1 = 0.39$ and $C_2 = 0.232$ are obtained as fitting parameters to the experimental data. Although these relations are clearly different, they predict somewhat similar values. The recombination rate given by Eq. (1) is approximately 2.7 times larger (at $T \approx 7500$ K) than the corresponding rate given by Eq. (2), while in the case of the ionisation rate, the first formula predicts higher rates by 1.13, for the same value of temperature as before.

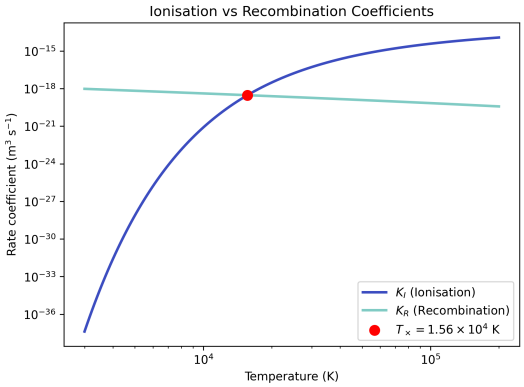

Fig. 1. Variation in the ionisation (K_I) and recombination (K_R) rates with temperature in the solar atmosphere.

In our study we employed the rates given by Eq. (1). These rates do not include photo-ionisation or ionisation from excited states, which are known to be important in the chromosphere. Ballai et al. (2024) have shown that, depending on the temperature of particles, these two rates can be rather different. While for low temperatures the recombination is the dominant process, for larger values of the temperature, ionisation is the process that is able to change the chemical composition of the plasma.

Figure 1 shows how the ionisation rate (K_I) and recombination rate (K_R) vary with temperature for conditions typical of the solar atmosphere. The ionisation rate rises steeply as the temperature increases, reflecting the fact that energetic collisions at higher temperatures are far more effective at removing electrons from atoms. In comparison, the recombination rate changes much more gradually and even decreases slightly, since recombination becomes less efficient when particles carry more thermal energy. The point where the two curves meet, around $T_x = 1.56 \times 10^4$ K, marks the temperature at which ionisation and recombination act with similar strength. Below this temperature, recombination dominates, and the plasma tends to remain weakly ionised, whereas above it, ionisation takes over and the ion fraction can rise quickly. This transition is highly relevant to chromospheric and transition-region plasmas, where small temperature changes can noticeably shift the ionisation balance, influencing wave propagation and damping. At photospheric and lower-chromospheric temperatures, recombination generally dominates over ionisation, maintaining a low equilibrium charge density despite the presence of magnetic fields. The high particle densities ensure that collisional timescales between species are short, leading to strong momentum and thermal coupling between ions, electrons, and neutrals, even though only the charged component interacts directly with the magnetic field.

Since the lengths we considered are much greater than the Debye length, we assumed that the condition of quasi-neutrality is satisfied, i.e. in equilibrium, the number density of positive ions and electrons is identical. The ionisation reaction takes place when a neutral hydrogen atom and an electron with energy larger than the ionisation energy collide, and the ionisation rate of neutrals is given as

$$\Gamma_i^{\rm ion} = n_n n_e K_I = n_n n_i K_I, \tag{3}$$

where n_n and n_i are the number densities of neutrals and electrons (ions). Similarly, the recombination is understood as the result of collisions of positive protons and electrons:

$$\Gamma_n^{\rm rec} = n_i n_e K_R = n_i^2 K_R. \tag{4}$$

These terms serve as source and sink terms in the mass conservation equations for ions and neutrals.

We should note, however, that in the real chromosphere, photo-ionisation is not merely a small correction. Hydrogen ionisation is known to be strongly non-local thermodynamic equilibrium, and radiation in the Balmer continuum can make a major contribution to the hydrogen rate system (Carlsson & Stein 2002; Leenaarts et al. 2007). That is why the present approach, which includes only collisional ionisation and radiative recombination, should be regarded as an idealised baseline model. The omission of photo-ionisation is expected to affect the results quantitatively rather than qualitatively. In particular, it could increase the effective ionisation rate, shorten the chemical relaxation timescales, and shift the precise damping rates and boundaries between propagating, non-propagating, and over-damped regimes. It can also alter the effective ionisation fraction by increasing the charged component in parts of the chromosphere. Nevertheless, the central result of the present work should remain robust even when a more complete radiative treatment is included.

This regime cannot be adequately described by single-fluid MHD and instead requires a multi-fluid approach that accounts explicitly for ionisation-recombination effects and collisional coupling. We considered a homogeneous magnetic field oriented along the z-axis and a two-dimensional dynamics in the xz plane. The plasma was treated as a two-fluid system, where the charged fluid (denoted by an index i) and the neutral fluid (denoted by an index n) interact through short-range collisions. In equilibrium, the plasma was considered to be uni-thermal (all species having the same temperature). This assumption is very easy to satisfy, as Alharbi et al. (2021) have shown that the thermalisation of the plasmas occurs in a few collisional times.

The spatio-temporal evolution of the plasma and its interaction with the magnetic field can be described by the system of two-fluid MHD equations:

$$\frac{\partial \rho_i}{\partial t} + \nabla \cdot (\rho_i \mathbf{v}_i) = m_i(\Gamma_i^{\rm ion} + \Gamma_i^{\rm rec}), \tag{5}$$

$$\frac{\partial \rho_n}{\partial t} + \nabla \cdot (\rho_n \mathbf{v}_n) = m_n(\Gamma_n^{\rm ion} + \Gamma_n^{\rm rec}), \tag{6}$$

$$\rho_i \frac{\partial \mathbf{v}_i}{\partial t} + \nabla \cdot (\rho_i \mathbf{v}_i \cdot \mathbf{v}_i + p_i) = \frac{[(\nabla \times \mathbf{B}) \times \mathbf{B}]}{\mu_0} + m_i \mathbf{v}_n \Gamma_i^{\rm ion} - m_i \mathbf{v}_i \Gamma_n^{\rm rec} + \mathbf{R}_{in}, \tag{7}$$

$$\rho_n \frac{\partial \mathbf{v}_n}{\partial t} + \nabla \cdot (\rho_n \mathbf{v}_n \cdot \mathbf{v}_n + p_n) = m_i \mathbf{v}_i \Gamma_n^{\rm rec} - m_i \mathbf{v}_n \Gamma_i^{\rm ion} - \mathbf{R}_{in}, \tag{8}$$

$$\frac{\partial \mathbf{B}}{\partial t} = \nabla \times (\mathbf{v}_i \times \mathbf{B}), \quad \nabla \cdot \mathbf{B} = 0, \tag{9}$$

$$\frac{\partial \epsilon_i}{\partial t} + \nabla \cdot (\epsilon_i \mathbf{v}_i + \mathbf{v}_i p_i) = \mathbf{j} \cdot \mathbf{E} + \mathbf{v}_i \cdot \mathbf{R}_i^{in} + Q_i^{in} - \frac{1}{2} m_i v_i^2 \Gamma_n^{\rm rec} - Q_n^{\rm rec} + \Gamma_i^{\rm ion} \left(\frac{1}{2} m_i v_n^2 - \Phi \right) + Q_i^{\rm ion}, \tag{10}$$

$$\frac{\partial \epsilon_n}{\partial t} + \nabla \cdot (\epsilon_n \mathbf{v}_n + \mathbf{v}_n p_n) = -\mathbf{v}_n \cdot \mathbf{R}_i^{in} + Q_n^{ni} - \frac{1}{2} m_i v_n^2 \Gamma_i^{\rm ion} - Q_i^{\rm ion} + \frac{1}{2} m_i v_i^2 \Gamma_n^{\rm rec} + Q_n^{\rm rec}, \tag{11}$$

with $\Gamma_i^{\rm ion} = -\Gamma_n^{\rm ion}$ and $\Gamma_i^{\rm rec} = -\Gamma_n^{\rm rec}$, $\epsilon_\alpha = \rho_\alpha v_\alpha^2/2 + p_\alpha/(\gamma - 1)$ is the internal energy density of fluid α, with $\gamma = 5/3$ being the

adiabatic index, $\mathbf{R}_{in}$ is the momentum exchange between colliding ions and neutrals that preserves the identity of particles and it is given as

$$\mathbf{R}_{in} = m_{in} n_i \nu_{in} (\mathbf{v}_n - \mathbf{v}_i),$$

with $m_{in} = m_i m_n/(m_i + m_n) \approx m_i/2$ is the centre of momentum mass. In the above equations $Q_\alpha^{\alpha\beta}$ is the frictional and thermal heating of species α due to the interaction with species β and it is given by

$$Q_\alpha^{\alpha\beta} = \mathbf{R}_\alpha^{\alpha\beta} \cdot (\mathbf{v}_\beta - \mathbf{v}_\alpha) + \frac{3}{2} \nu_{\alpha\beta} n_\alpha k_B (T_\beta - T_\alpha).$$

The terms $Q_i^{\rm ion} = 3/2 k_B T_n \Gamma_i^{\rm ion}$ and $Q_n^{\rm rec} = 3/2 k_B T_i \Gamma_n^{\rm rec}$ are the thermal energy gains of ions and neutrals due to ionisation and recombination, respectively. $T_i = p_i/n_i k_B$, $T_n = p_n/n_n k_B$ are the temperatures of ions and neutrals. The term containing the ionisation energy of the hydrogen, Φ, denotes the loss of the internal energy of charged particles due to the radiation generated in the process of ionisation. The above system of equations is closed by the relevant Maxwell equations:

$$\mathbf{j} = \nabla \times \mathbf{B}, \quad \mathbf{E} = -\mathbf{v} \times \mathbf{B}, \quad \nabla \mathbf{E} = -\frac{\partial \mathbf{B}}{\partial t}.$$

In the induction equation, Eq. (9), we neglected resistive effects as these are less relevant when compared to the collisional transfer of momentum. The validity of this statement should be revisited if transversal inhomogeneities in the plasma are assumed, and the existence of large field gradients that can enhance the importance of resistive terms in the induction equation.

The complexity of the above system of equations can be considerably reduced by assuming small amplitude changes of the equilibrium (linear approximation); therefore, we write all physical quantities as the sum between their equilibrium values (denoted by an index *0*) and perturbations such that perturbations are considered to be much smaller than their equilibrium values. As a consequence, terms containing squares or products of perturbations can be neglected. The equilibrium is assumed to be homogeneous, stationary and static ($v_{0i} = v_{0n} = 0$). In addition, we considered that the equilibrium state is in ionisation equilibrium; therefore, from Eqs. (5) and (6) we can write

$$\frac{n_{0n}}{n_{0i}} = \frac{K_R}{K_I} = \chi, \tag{12}$$

which constitutes the ionisation factor of the system. The parameter χ is going to play a key role in our discussion, as its value relative to one would help us classify the nature of the plasma and the dominant process that acts to change the chemical composition of the plasma. Since our study deals with weakly ionised plasmas, in the remaining part of our study we focused on the case when $\chi > 1$. This particular choice also implies that recombination is dominant.

As a result of the linearisation, the system of governing equations transforms into

$$\left(\frac{\partial}{\partial t} - n_{0n} K_I + 2 n_{0i} K_R\right) n_i + n_{0i} \nabla \cdot \mathbf{v}_i - n_{0i} n_n K_I = 0, \tag{13}$$

$$\left(\frac{\partial}{\partial t} + n_{0i} K_I\right) n_n + n_{0n} \nabla \cdot \mathbf{v}_n - (2 n_{0i} K_R - n_{0n} K_I)\, n_i = 0, \tag{14}$$

$$\left(\frac{\partial}{\partial t} + \frac{\nu_{in}}{2} + n_{0i} K_R\right) \mathbf{v}_i - \left(\frac{\nu_{in}}{2} + n_{0n} K_I\right) \mathbf{v}_n + \frac{1}{m_i n_{0i}} \left[\nabla p_i - \frac{(\nabla \times \mathbf{b}) \times \mathbf{B}_0}{\mu_0}\right] = 0, \tag{15}$$

$$\left(\frac{\partial}{\partial t} + \frac{\nu_{in}}{2\chi} + n_{0i} K_I\right) \mathbf{v}_n - \left(\frac{\nu_{in}}{2\chi} + \frac{K_R n_{0i}}{\chi}\right) \mathbf{v}_i + \frac{\nabla p_n}{m_i n_{0n}} = 0, \tag{16}$$

$$\frac{\partial \mathbf{b}}{\partial t} - \nabla \times (\mathbf{v}_i \times \mathbf{B}_0) = 0, \tag{17}$$

$$\frac{1}{\gamma - 1}\left(\frac{\partial p_i}{\partial t} + \rho_{0i} c_{Si}^2 \nabla \cdot \mathbf{v}_i\right) = \frac{3}{2} n_{0i} k_B \nu_{in} (T_n - T_i) - \Phi K_I n_{0i} (n_n + \chi n_i) + \frac{3}{2} k_B T_0 n_{0i} (n_n K_I - n_i K_R) + \frac{3}{2} k_B n_{0i}^2 (\chi K_I T_n - K_R T_i), \tag{18}$$

$$\frac{1}{\gamma - 1}\left(\frac{\partial p_n}{\partial t} + \rho_{0n} c_{Sn}^2 \nabla \cdot \mathbf{v}_n\right) = \frac{3}{2} n_{0i} k_B \nu_{in} (T_i - T_n) + \frac{3}{2} k_B T_0 n_{0i} (n_i K_R - n_n K_I) + \frac{3}{2} k_B n_{0i}^2 (K_R T_i - \chi K_I T_n), \tag{19}$$

together with the perturbations of temperatures (derived from the linearised ideal gas law for ions and neutrals)

$$T_i = \frac{p_i}{n_{0i} k_B} - \frac{n_i}{n_{0i}} T_0, \quad T_n = \frac{p_n}{n_{0n} k_B} - \frac{n_n}{n_{0n}} T_0, \quad T_0 = \frac{m_i c_{Si}^2}{\gamma k_B}.$$

Since our aim was to investigate waves propagating in partially ionised plasmas in ionisation non-equilibrium, we took all variables to be proportional to the exponential factor $e^{i(\omega t - k_x x - k_z z)}$, where $\mathbf{k} = (k_x, 0, k_z)$ is the wavevector and ω is the complex frequency. The real part of ω describes the frequency of waves, while the imaginary part denotes the damping rate of waves. As a consequence of this ansatz, the temporal and spatial derivatives in the linearised system of equations will be replaced as $\partial/\partial t \to i\omega$ and $\nabla \to -i\mathbf{k}$. The above setup describes a magnetoacoustic mode propagating at an arbitrary angle with respect to the ambient magnetic field. To assess the consequences of various propagation directions, we write the wavevector as $\mathbf{k} = (k \sin\alpha, 0, k \cos\alpha)$, where now α is the angle between the propagation direction and the equilibrium magnetic field.

3. Dispersion relation

After Fourier analysing the perturbations that appear in Eqs. (13)–(19), the MHD equations can be reduced to a system of equations of the form

$$\sum_{j=1}^{8} A_{ij}(\omega, \mathbf{k})\, Y_j = 0, \qquad i = 1, \ldots, 8, \tag{20}$$

where the eigenfunction vector, $\mathbf{Y}$ is defined in terms of the dimensionless quantities

$$Y = \left(\tilde{n}_i \quad \tilde{n}_n \quad u_{ix} \quad u_{nx} \quad u_{iz} \quad u_{nz} \quad \tilde{p}_i \quad \tilde{p}_n\right). \tag{21}$$

The dimensionless quantities that appear in the expression of Y are defined as

$$\tilde{n}_i = \frac{n_i}{n_{0i}}, \quad \tilde{n}_n = \frac{n_n}{n_{0n}}, \quad u_{ix} = \frac{v_{ix}}{v_A}, \quad u_{iz} = \frac{v_{iz}}{v_A},$$

$$u_{nx} = \frac{v_{nx}}{v_A}, \quad u_{nz} = \frac{v_{nz}}{v_A}, \quad \tilde{p}_i = \frac{p_i}{p_{0i}}, \quad \tilde{p}_n = \frac{p_n}{p_{0n}}.$$

The explicit expressions of the matrix elements A_{ij}, together with a brief derivation sketch linking each matrix row to the Fourier-analysed linearised equations, are given in the appendix.

The homogeneous system of equations, Eq. (20), will admit solutions provided the determinant of the matrix A_{ij} is zero, which constitutes the dispersion relation of our problem. Due to the collisions between particles as well as thermal exchange between species, the roots of this dispersion relation are complex. The dispersion relation describes three forward and backward propagating waves and two so-called entropy modes. The entropy mode is a mode whose frequency is purely imaginary and describes a non-propagating, evanescent mode. In the dimensionless system of equations, we write the dimensionless frequency and collisional frequency in terms of the Alfvén frequency, kv_A, i.e.

$$\Omega = \frac{\omega}{kv_A}, \quad X = \frac{\nu_{in}}{kv_A}. \tag{22}$$

In addition, we used the following dimensionless quantities:

$$P = \frac{n_{0i}K_I}{kv_A}, \quad \beta = \frac{2c_{Si}^2}{\gamma v_A^2}, \quad \hat{\Phi} = \frac{\Phi}{m_i c_{Si}^2}. \tag{23}$$

The obtained dispersion relation will be analysed in the next section by finding roots of the dispersion relation using a numerical approach.

The parameter values considered in our study are not meant to correspond to one specific height in the solar atmosphere, but rather to represent a range of physical regimes that can occur in weakly ionised chromospheric plasma. In the context of the VAL-C quiet-Sun model, $\chi = 2$ can be regarded as a representative weakly ionised state in which neutrals still dominate the inertia, while the charged component remains dynamically important. The values $\beta = 0.1$ and $\beta = 10$ are chosen to bracket magnetically dominated and gas-pressure-dominated conditions, respectively. Similarly, the dimensionless quantity X measures the relative importance of collisions and wave dynamics, so that $X = 0.1$ and 5 represent weakly and strongly coupled regimes. Since X depends not only on the local plasma conditions but also on the wave scale, these values should be interpreted as representative chromospheric dynamical regimes rather than as values tied uniquely to a single VAL-C height.

4. Results

To investigate the behaviour of magnetoacoustic waves in partially ionised solar plasmas, it is essential to employ a diagnostic tool capable of simultaneously visualising the angular dependence of the wave frequency and the influence of dissipative processes introduced by the collisional damping, as well as the effects of ionisation–recombination and the dynamics of waves. For this purpose, Friedrichs diagrams (also known as polar phase speed diagrams) provide a particularly powerful and intuitive method of representation. Unlike traditional dispersion plots that illustrate the variation of frequency with wavenumber along a single propagation direction, Friedrichs diagrams map the real and imaginary parts of the wave frequency as a function of the propagation angle relative to the magnetic field. This allows the complete directional propagation properties of individual MHD modes to be assessed in a single figure.

The value of Friedrichs diagrams becomes especially clear in partially ionised media, where ion–neutral coupling, collisional damping, and dynamic ionisation and recombination can significantly modify wave behaviour. These mechanisms can introduce angular cutoffs, change the effective phase speed of slow and fast modes, or shift the dominant restoring force from magnetic tension to gas pressure, depending on plasma parameters. Friedrichs diagrams provide a direct visual means to identify such transitions, showing where the real part of the frequency decreases to zero (signalling a change from propagating to evanescent behaviour) and how damping rates vary with angle.

In this context, Friedrichs diagrams therefore serve not only as a presentation tool, but as an interpretative framework through which the effects of ionisation fraction, collisional frequency, modification of the chemical composition of the plasma, and plasma-β on magnetoacoustic wave propagation can be analysed. They allow the slow and fast branches to be followed continuously from parallel to perpendicular propagation, making angular cutoffs and the evolution of mode character explicit.

Given the large number of parameters that can influence the properties of waves, we are going to discuss several cases relevant to the partially ionised solar atmospheric plasma. Accordingly, we discuss the cases for weakly and strongly collisional plasmas separately, as well as the cases where plasma-β is less than or greater than 1. To make the distinction between oscillatory and strongly damped behaviour more precise, we used the ratio $R = Im(\Omega)/Re(\Omega)$. When $R < 1$, the mode remains oscillatory, whereas $R > 1$ indicates that damping dominates over oscillation and the mode can be regarded as effectively over-damped. In the limiting case $Re(\Omega) = 0$, the mode becomes purely non-propagating.

4.1. Weakly collisional plasma

The real (top panel) and imaginary (bottom panel) values of the dimensionless frequency, Ω, with respect to the propagation angle are shown in Fig. 2. We considered a weakly collisional plasma ($X = 0.1$ as a representative value) and $\beta = 0.1$. Here, and in all subsequent plots, the fast magnetoacoustic mode is represented by blue lines, the neutral slow mode (acoustic mode) is indicated by green, while the ion slow mode is shown in orange. The results shown in this figure were obtained assuming that the plasma is in ionisation equilibrium, i.e. the ionisation and recombination rates are set to zero. These results will serve as a benchmark to all subsequent results, evidencing the effects of ionisation and recombination processes on wave propagation and damping.

For this set of parameters, the dispersion relation exhibits three clearly separated branches reflecting weak ion–neutral coupling. The real part of the solutions shows that in the partially ionised solar plasma discussed here, fast waves propagate with the largest speed (or frequency) and their propagation is isotropic. This result is easy to understand, as for low values of plasma-β fast magnetoacoustic waves propagate at roughly the Alfvén speed and are only weakly angle-dependent. These waves are mostly driven by magnetic tension.

The two other modes (ion and neutral slow modes) propagate with much lower speeds. While the neutral slow mode (or acoustic mode) shows, again, an isotropic angular variation, the ion slow mode behaves like an ordinary MHD mode, i.e. the largest speed is attained for parallel propagation ($\alpha = 0, \pi$), and these waves cannot propagate across the field.

The damping rate of waves shown in the right-hand side panel of Fig. 2 follows the angular pattern of the real part of solutions, and all three waves undergo a weak damping in the sense that $Im(\Omega) < Re(\Omega)$. Fast waves have a very isotropic damping rate and, in terms of the magnitude, fast waves survive for a longer time than ion slow modes. The ion slow modes have the largest damping rate, and it is very angle-dependent, similar to the real part of the solutions corresponding to this mode. This pattern is rather intuitive for slow modes propagating in a low-β

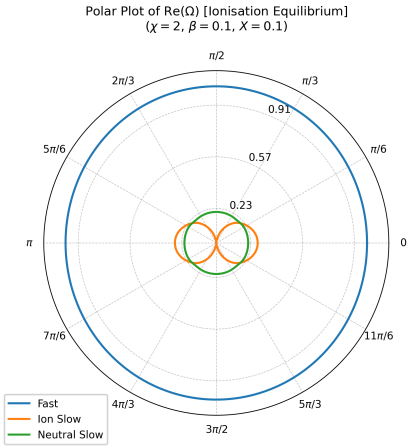

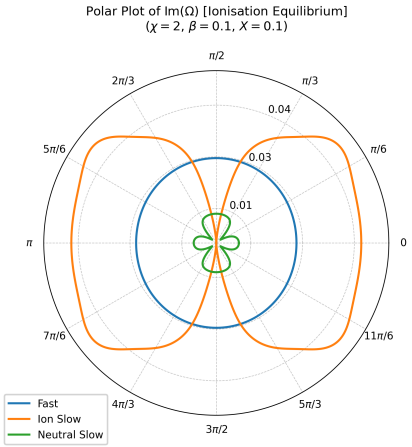

Fig. 2. Friedrichs diagrams corresponding to real (*top*) and imaginary (*bottom*) part of the dimensionless frequency of waves (in units of the Alfvén frequency) for fast waves (blue), ion slow modes (amber), and neutral slow modes (green) with the propagation angle, α. The values of the parameters used for these plots are shown on each diagram. These plots are valid for a plasma in ionisation equilibrium.

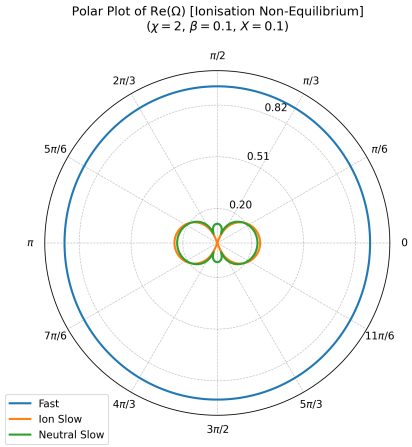

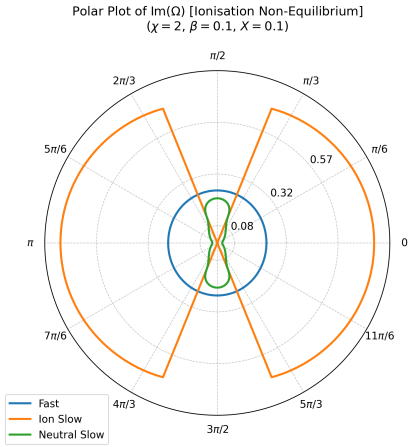

Fig. 3. Same as Fig. 2 but including the angular variation of the dimensionless frequency and damping rate of magnetoacoustic modes in the case of non-equilibrium ionisation in a weakly collisional plasma.

plasma. Now, the ion slow mode is essentially an acoustic-like compressive mode guided along the magnetic field. In weakly collisional plasma, the coupling between ions and neutrals is not perfect, so the slow wave drives significant ion–neutral drift and frictional heating, resulting in strong damping. The neutral slow mode has the smallest damping rate, a result that is easy to understand given the weakly ionised character of the plasma. The angular variation of the damping rate of this mode shows a small four-lobed pattern, which is a result of how the neutrals and ions are coupled in the plasma we investigated, as well as how efficiently a neutral acoustic motion excites ion motion along and across the magnetic field. The damping rate of neutral waves comes from the ion–neutral friction term, in which the ion velocity perturbation induced by a neutral wave is small, but it is strongly anisotropic. The way these velocity perturbations couple when waves propagate along and across the field gives rise to an observable difference in the damping rate of these waves in the parallel and perpendicular directions. The four minima that appear in the damping rate of neutral waves at intermediate propagation angles are the results of parallel and perpendicular ion responses partially cancelling the ion–neutral drift, minimising frictional dissipation.

When ionisation and recombination processes are taken into account, the angular variation of the real (top panel) and imaginary (bottom panel) parts of the frequency is shown in Fig. 3. First of all, we should note that the frequency of all waves is reduced by the modifications in the chemical composition of the plasma, which serves as an additional channel for momentum transfer between species. As expected, the angular dependence of the dimensionless frequency of fast waves is not modified by the presence of changes in the chemical composition of the plasma. In the low plasma-β regime, these waves are driven mostly by magnetic tension, and they are not as sensitive to compressibility and chemical composition of the plasma as slow and acoustic modes. Slow magnetoacoustic modes attached to the charged species have a similar behaviour as in the case of ionisation equilibrium, i.e. they are anisotropic, showing the largest frequency when propagating along the field, while the propagation across the field is completely suppressed. On the other hand, neutral slow waves display a very different variation of their dimensionless frequency. In contrast to the result we obtained in equilibrium, the variation of the frequency is no longer isotropic and to a large extent it mimics the variation of the ion slow waves. Although the collisional coupling is weak, ionisation and recombination couple the neutral density and pressure perturbations to the charged component's compressions, and the charged compressions are anisotropic because of the magnetic field. As a result, the neutral slow mode inherits anisotropy from the magnetised component through chemistry, not through friction. Other than perpendicular propagation, the green and orange radii are very close (nearly the same phase speed), which means that the two slow branches become more mixed, and these

are less purely species-separated when chemical variations are allowed.

The damping rates of the three modes in the presence of ionisation and recombination show a different pattern compared to the equilibrium case. In the case of fast waves, the damping rate of these waves is isotropic, but its magnitude is somewhat smaller than the equilibrium one, which means that ionisation and recombination slightly reduces fast-mode damping in this weak-coupling regime. Slow waves associated with ions display the largest damping rate, and it is clear that ionisation and recombination processes introduce an additional coupling and relaxation timescale that makes the damping rate of ion slow modes have a sharper angular cutoff. The damping rate of neutral slow modes shows the most different behaviour compared to the equilibrium case. First of all, the damping rate stays rather anisotropic, with waves propagating in a perpendicular direction to the ambient magnetic field having the largest damping rate, and this change is due solely to the modifications in the chemical composition of the plasma. In non-equilibrium, the damping of the neutral mode becomes controlled less by pure ion–neutral friction and more by how strongly the mode drives composition changes at a given angle. For parallel propagation, the neutral slow mode excites the ion slow mode, which propagates efficiently along the magnetic field and allows a partial co-motion of ions and neutrals. This reduces ion–neutral drift and hence frictional damping. For perpendicular propagation, the ion slow mode is non-propagating, ions remain nearly stationary, and neutral motion produces maximal drift and damping. We should also note that modifications in the chemical composition of the plasma are changing the damping character of waves. While fast waves remain weakly damped (as in the case of ionisation equilibrium), slow waves associated with charges and neutrals undergo over-damping, so these modes are very effectively damped. For this set of parameters, the inclusion of ionisation and recombination increases the damping of the slow branches to the point where $R > 1$, whereas in ionisation equilibrium these modes remain oscillatory. This shows that chemical relaxation can itself drive the system into an over-damped regime.

To provide a rough connection with observables, the dimensionless damping rates can be converted into physical damping times using $\tau_D = 1/Im(\Omega k v_A)$, and into damping lengths through $L_d = v_{ph}\tau_D = Re(\Omega)/k\ Im(\Omega)$. For the representative non-equilibrium case shown in Fig. 3, namely $\chi = 2, \beta = 0.1$ and $X = 0.1$, and adopting the chromospheric values $v_A = 100$ km s^{-1} and $\lambda = 500$ km, we obtain $kv_A = 1.26$ s^{-1}. From Fig.3 we see that weakly damped fast waves have $Im(\Omega) = 0.01 - 0.03$, which corresponds to damping times of the order of 25–80 s, and damping lengths of the order of $(2.5{-}8) \times 10^3$ km. For these values $P/\tau_D \sim 5{-}15$, where P is the period of waves. In contrast, the slow branches are much more strongly damped and can become effectively over-damped, suggesting that they would be considerably more difficult to detect directly. These values are consistent with chromospheric wave observations: compressive chromospheric disturbances with phase speeds of the order of 48–270 km s^{-1} and periods of the order of a few minutes have been reported (Morton et al. 2012). Finally, the damping times predicted by our analysis are of the same order as the values determined from IRIS observations (Yuan et al. 2026).

4.2. Strongly collisional plasma

As an illustrative figure, in this section, we consider $X = 5$ to represent a strongly collisional plasma. Figure 4 shows the real and imaginary parts of the solutions of the dispersion relation when the collisional rate is high, and ionisation and recombination processes are not taken into account. In contrast to the weakly collisional case, in this case, the frequent collisions between charges and neutrals efficiently couple the two species, resulting in suppressed relative drift. As a result, independent neutral acoustic motion is no longer possible, as this is absorbed into a collective compressive mode of the combined charged fluid. It is clear that the frequencies of the waves are smaller compared to the weakly collisional case, a result that confirms the earlier findings by Soler et al. (2013). Fast modes continue to be dominated by magnetic tension; they have a large phase speed ($\sim v_A$) and involve relatively small compressive density perturbations. That is why, for these modes, collisions between particles mostly act to slightly re-normalise inertia; however, they do not introduce anisotropy. Secondly, the damping rate of fast waves is larger when they propagate parallel to the magnetic field, i.e. in the direction where the propagation speed of slow waves takes its maximum value. In the case of parallel propagation, the Lorentz force does not provide a restoring force that can deflect the motion. That is why the fast branch becomes more like a longitudinal magnetosonic oscillation, so the velocity tends to line up more with k. This makes the compressibility ($\nabla \cdot \mathbf{v}$) and density perturbations stronger. In the case of perpendicular propagation, the fast wave is more strongly associated with field-line bending and transverse motion, as well as a smaller compressive part.

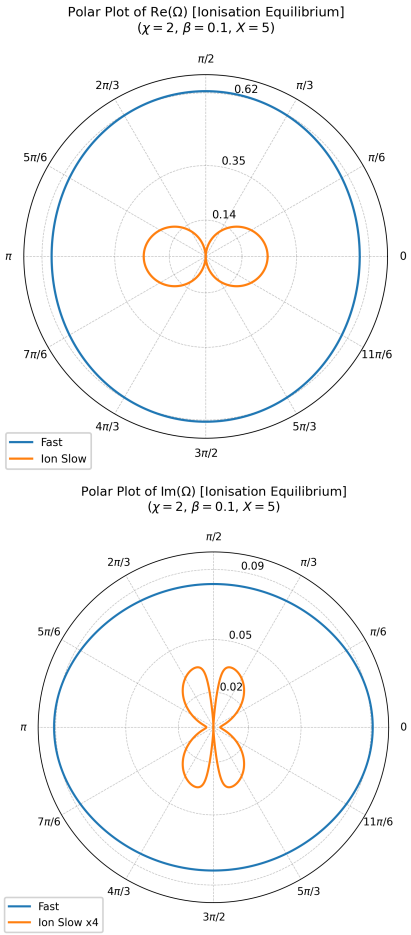

Fig. 4. Same as Fig. 2 but for a strongly collisional plasma. The magnitude of the imaginary part corresponding to ion slow waves has been magnified four-fold for visualisation purposes.

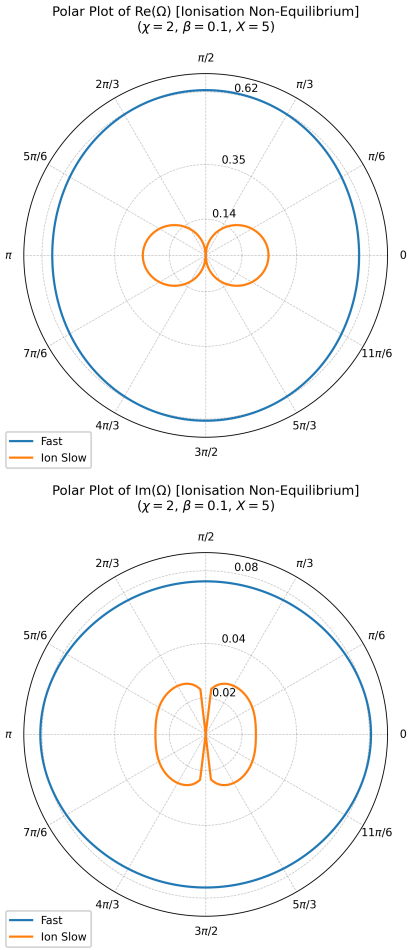

Fig. 5. Angular dependence of wave modes in ionisation non-equilibrium (similar to Fig. 4).

The damping rate of all modes shows that these waves are weakly damped. The damping rate of ion slow mode (or collective mode) is very low, and for illustration, this quantity has been magnified uniformly by a factor of 4 (see the lower panel of Fig. 4). As the collisions are rather strong, the drift velocity of the two species is small; the damping now is provided mainly by the collisional thermal exchange between species. For slow modes propagating parallel to the ambient magnetic field for small values of plasma-β, the effect of compressions is strong in both fluids, but ions and neutrals are tightly locked; therefore, their temperature perturbations tend to be similar, resulting in a weak thermal exchange damping.

In the case of perpendicular propagation, although the two species are tightly coupled, the presence of the magnetic field will prevent slow modes from propagating across the field. At intermediate angles, we obtain the largest mismatch in the partitioning of compression and heating between the ion and neutral internal energies, because the slow wave has a mix of magnetic and acoustic character that can lead to a maximum mismatch between the temperatures of ions and neutrals, i.e. a maximised damping rate.

The two panels of Fig. 5 display the real and imaginary parts of possible waves propagating in a partially ionised, collisionally dominated plasma when ionisation and recombination effects are taken into account. In the strong collisional limit, the traditional damping mechanism that is proportional to the drift velocity is very small and ionisation and recombination introduces a new irreversible dissipation mechanism that does not require a large drift to dissipate energy. The upper panel shows that, despite changes in the chemical composition of the plasma being taken into account, the frequency of waves is not modified, suggesting that ionisation and recombination are just second-order effects compared to collisions. All modes are dampened with weak damping, and the damping rates are somewhat lower than in the ionisation equilibrium. The damping rate of fast waves is not modified by the changes in the chemical composition of the plasma; however, as in the case of ionisation equilibrium, the damping rate is larger in the parallel direction. This confirms the fact that the damping of fast waves is primarily due to the collisional thermal damping and not because of the changes in the chemical composition of the plasma.

The damping rate of the charged fluid shows a distinctively different pattern compared to the equilibrium case. First of all, the magnitude of the damping rate is approximately four times larger, and this can be attributed solely to the ionisation and recombination processes that add a strong energy sink that acts efficiently on compressions. Parallel to this, chemical changes in the plasma tend to smooth the strong anisotropy in the damping rate of slow waves. The increase in the number of neutrals at the expense of ions increases the compressibility of the plasma. For parallel propagation, the slow mode is essentially a field-aligned acoustic oscillation of the coupled mixture. In the presence of a relatively small drift, the damping of waves is small. As the propagation angle increases, the slow mode acquires additional magnetic pressure coupling, producing stronger phase lags between species, which slightly increases the friction, as well as the thermal and chemical relaxation, leading to an increase in the damping rate. Near $\alpha = \pi/2$, the slow mode loses its propagating nature, and the oscillatory driver for damping vanishes.

4.3. The effect of plasma-β

We next investigated the effect of plasma-β on the propagation and damping of waves in a partially ionised plasma. By increasing β, the plasma changes from a magnetically dominated regime to one in which thermal pressure plays a central role, leading to a qualitative change in the nature of magnetoacoustic modes. In this case, the fast mode becomes increasingly acoustic and nearly isotropic, while the slow mode remains strongly guided by the magnetic field. These changes modify the relative importance of ion–neutral coupling, compressibility, and dissipative processes, and therefore have a direct impact on the angular dependence of wave propagation and damping.

Figure 6 shows the real and imaginary parts of the solutions of the dispersion relation in ionisation equilibrium. For $\beta = 10$ and weak collisional coupling ($X = 0.1$), the magnetoacoustic spectrum undergoes a clear reorganisation. The fast mode becomes predominantly acoustic and nearly isotropic, while the ion slow mode remains strongly field-aligned with a reduced phase speed. A distinct neutral acoustic mode persists, reflecting the weak coupling between species. Compared to the low plasma-β case, the frequency of waves is larger thanks to the stronger compressional character of the plasma. Damping is dominated by neutral–ion friction acting on the neutral slow mode, which exhibits the largest attenuation and only weak angular dependence. In contrast, both fast and ion slow modes remain weakly damped, highlighting that compressibility alone is insufficient to produce strong dissipation in the absence of efficient collisional or chemical coupling.

In the presence of ionisation and recombination, the frequency of waves is smaller, suggesting that changes of the

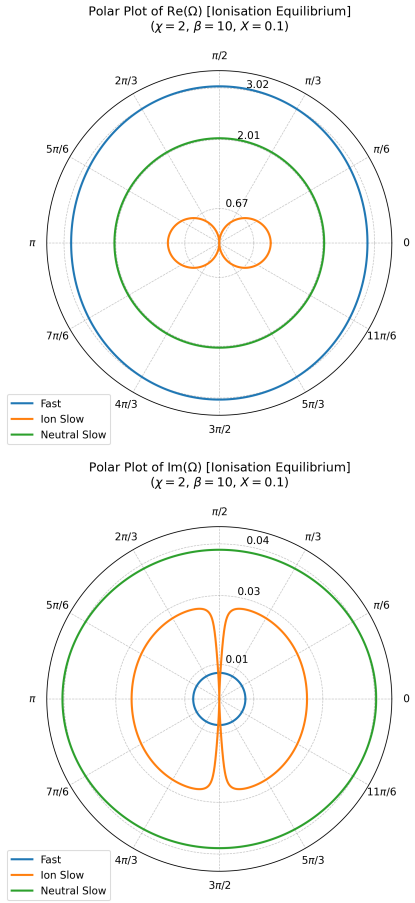

Fig. 6. Angular variation of the real (*top*) and imaginary (*bottom*) parts of the dimensionless frequency of magnetoacoustic modes propagating in a weakly ionised and weakly collisional plasma for $\beta = 10$. An elevated value of β means an enhanced compressibility of the plasma.

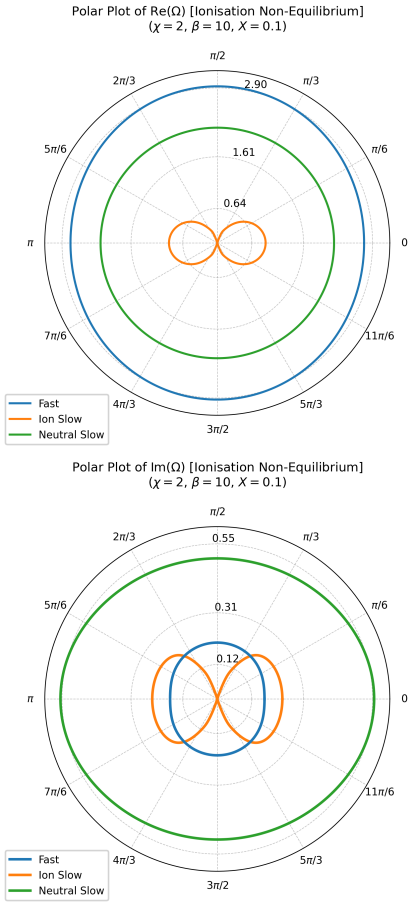

Fig. 7. Same as Fig. 6 but with the effects of ionisation and recombination taken into account.

chemical composition of the plasma act to reduce these values, i.e. they act as dissipation channels (bottom panel of Fig. 7). The damping of these waves undergoes a clear modification (top panel of Fig. 7). The neutral slow mode continues to have the largest damping rate; however, compared to the equilibrium case, the damping rate of these modes shows that they undergo heavier damping when they propagate along the magnetic field. Although the neutral slow mode is not directly constrained by the magnetic field, its damping depends on the response of the ionised component through collisions and chemical relaxation. For field-aligned propagation, ions can follow the compressive motion more efficiently, leading to enhanced momentum and energy exchange with neutrals and, consequently, slightly stronger damping. In contrast, for perpendicular propagation, the ion response is magnetically inhibited, reducing the efficiency of these dissipative processes.

In the equilibrium case, the ion slow mode had a damping rate that was larger than the damping rate of fast waves. In the presence of ionisation and recombination, these two rates become comparable, in the sense that the damping rate of ion slow modes is reduced, while the damping rate of fast waves is increased. In the non-equilibrium case, the ionisation and recombination processes seem to redistribute which mode carries the compressive or thermodynamic perturbations that chemistry can damp. In the investigated high-β plasma, the fast mode is the main compressive (acoustic-like) branch, while the slow mode becomes more magnetic or field-guided. The change in the chemical composition of the plasma therefore damps the fast branch more efficiently, but it can reduce the slow-mode damping by reducing ion–neutral drift and weakening the frictional damping that dominated in equilibrium. When comparing these results with the ones obtained for small β (see Fig. 3), it is clear that increasing the value of β shifts the chemical sensitivity of the system from the slow modes to the fast mode.

Finally, let us assess the effect of collisions on the properties of waves that can propagate in the partially ionised plasmas in the presence of chemical changes. Figure 8 shows the solutions of the dispersion relation for waves propagating in a collision-dominated plasma in ionisation equilibrium. For this case, we considered $\beta = 10$ and $X = 5$. The real part of the solutions shown in the upper panel reveals, first of all, that overall, collisions act to reduce the frequency of waves, a similar result as in the previous case. Fast waves show an isotropic behaviour, propagating at the combined sound speed of the ion–neutral mixture. The ion slow mode displays a clear two-lobed structure, with propagation confined to field-aligned directions. Its phase speed remains small compared to the fast mode, scaling roughly as $\cos\alpha$, suggesting that even in a pressure-dominated plasma, the slow mode remains magnetically guided and controlled by the Alfvénic response of the mixture. The neutral slow mode, having an intermediate propagation speed, shows a rather peculiar anisotropy, with waves propagating faster in the perpendicular direction. Since ion slow modes do not propagate across the field, ions provide limited magnetic resistance to compressions. Neutrals therefore oscillate closer to their natural acoustic speed. For parallel propagation, ions respond strongly along the

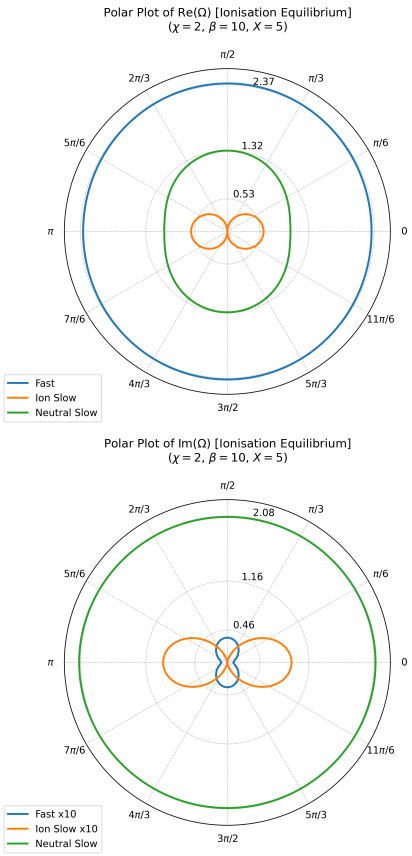

Fig. 8. *Top*: Same as Fig. 6 but for a strongly collisional plasma. *Bottom*: Damping rates of the fast and slow ion modes, magnified by a factor of 10 for clarity.

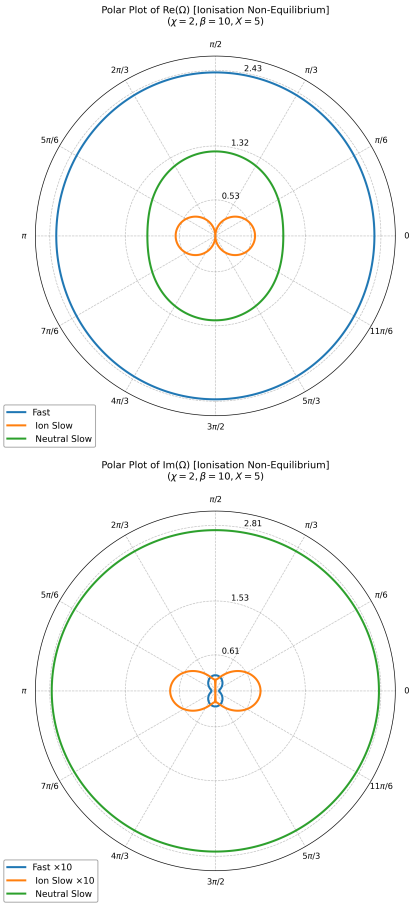

Fig. 9. Similar to Fig. 8 but also taking ionisation and recombination processes into consideration.

field and participate in slow-mode dynamics. In this situation, magnetic tension and pressure now oppose compressions. Since the plasma is strongly collisional, this magnetic stiffness is transferred to neutrals, resulting in a reduced phase speed.

The lower panel of Fig. 8 shows that despite the anisotropic behaviour of the phase speed, the damping rate of neutral slow modes is isotropic and has, by far, the largest damping rate. In the limit of strong collisional coupling, neutral acoustic energy is rapidly dissipated via ion–neutral friction and collisional thermal damping. Comparing the real and imaginary parts of the solutions for these modes, it is clear that neutral slow modes are over-damped, and the collisions act as a very effective damping mechanism. Since we are dealing with a strongly collisional plasma, the drift velocities are rather small, leading to a very low damping rate of fast and ion slow mode (for visualisation purposes, the rates of these two modes are magnified by a factor of 10). While the damping rate of ion slow modes preserves the anisotropy observed in the real part of this mode, the damping rate of fast modes is also anisotropic, showing a much larger damping rate when they are propagating perpendicular to the ambient magnetic field. This behaviour can be easily understood as the little dissipation this wave encounters is controlled by the small ion–neutral slippage, which is highly geometry-dependent, leading to the damping becoming strongly anisotropic.

The properties of the three waves when ionisation and recombination effects are taken into account are shown in Fig. (9). The angular variation of the real part of waves reveals that the ionisation non-equilibrium has no noticeable effect on the frequency of waves. Instead, the lower panel suggests that the ionisation non-equilibrium affects mainly the damping of waves. For fast waves, damping stays small (note the 10-fold magnification factor), but it is anisotropic with a clear enhancement towards more transverse directions. Compared to equilibrium, this is qualitatively similar in the sense that the damping of fast modes remains small, but the anisotropy tends to be more 'structured' once chemistry is included, since compressions now also perturb composition and temperature. For ion slow modes, the damping is also small in absolute terms (also needs a 10-fold magnification), but there is a region near the angles where the real part of the solutions is very small (approaching the perpendicular direction), where the mode is susceptible to becoming non-propagating (evanescent). The neutral slow mode shows an isotropic damping rate with the propagation angle, but more importantly, these waves are over-damped, and their lifetime is very short. The over-damping of the neutral slow mode does not contradict the weakly ionised nature of the plasma. Although neutrals dominate the mass density, the timescales associated with ion–neutral momentum and thermal exchange, and – when included – ionisation and recombination relaxation, are comparable to or shorter than the acoustic period of the neutral fluid. As a result, pressure perturbations cannot sustain oscillatory behaviour, and the neutral slow branch transitions into a strongly damped relaxation-type mode in both equilibrium and non-equilibrium regimes, with the latter further enhancing this effect through recombination-driven pressure loss. Comparing the real and imaginary parts of the neutral slow branch shows that $R > 1$ over the full angular range, both in ionisation equilibrium and in ionisation non-equilibrium. Therefore,

this mode is already effectively over-damped in the strongly collisional regime, and the inclusion of ionisation and recombination does not create the over-damped state, but instead modifies the detailed damping properties of an already strongly damped branch.

5. Conclusion

We have investigated the propagation and damping of magnetoacoustic waves in weakly ionised solar atmospheric plasmas using a two-fluid framework that explicitly accounts for ion–neutral collisions as well as ionisation and recombination processes. By extending previous equilibrium studies (e.g. Soler et al. 2013) to include ionisation non-equilibrium, we have shown that chemical relaxation introduces qualitatively new effects that cannot be captured by standard two-fluid or single-fluid descriptions.

Our analysis demonstrates that ionisation and recombination act as an additional dissipation channel that redistributes wave energy between species and modifies the relative damping efficiency of different wave branches. In weakly collisional plasmas, non-equilibrium effects primarily alter the slow and neutral acoustic modes, introducing anisotropy in their damping and coupling neutral dynamics more strongly to the magnetised ion component. In particular, neutral slow modes inherit magnetic anisotropy through chemistry rather than friction, while ion slow modes experience enhanced or suppressed damping depending on the propagation angle and plasma-β. Fast magnetoacoustic waves remain weakly damped in this regime, but their damping can be modified once chemical relaxation becomes comparable to collisional timescales.

In the strongly collisional limit, collisions efficiently lock ions and neutrals together, suppressing relative drift and eliminating independent neutral acoustic propagation in equilibrium. When ionisation and recombination are included, however, neutral slow modes persist as heavily damped, non-oscillatory relaxation modes. We find that these modes can become over-damped in both equilibrium and non-equilibrium cases, despite the plasma being weakly ionised. This behaviour arises because the combined effects of momentum exchange, thermal coupling, and chemical relaxation operate on timescales shorter than the neutral acoustic period, preventing sustained oscillations. Importantly, non-equilibrium chemistry further enhances this over-damping by introducing pressure and energy sinks associated with recombination.

The role of plasma-β is shown to be central in determining which wave branch is most affected by non-equilibrium processes. At low β, chemical effects primarily influence slow modes, while at high β the fast mode becomes increasingly compressive and therefore more susceptible to damping through ionisation recombination. This shift explains why fast-mode damping increases in high-β plasmas when non-equilibrium effects are included, while slow-mode damping can be reduced compared to equilibrium predictions.

Our results demonstrate that ionisation non-equilibrium fundamentally alters the angular dependence, damping hierarchy, and even the qualitative nature of magnetoacoustic modes in partially ionised plasmas. These findings highlight the importance of incorporating modifications of chemistry when modelling wave propagation and energy dissipation in the solar chromosphere and other weakly ionised astrophysical environments. In a subsequent study, we will focus on the strongly ionised plasma (the upper part of the chromosphere), where the process of ionisation is dominant.

Acknowledgements. JA acknowledges Shaqra University and the Ministry of Education in the Kingdom of Saudi Arabia for their financial support. IB, VF, and GV are grateful to the Science and Technology Facilities Council (STFC) grants ST/V000977/1, ST/Y001532/1. VF, GV thank the Institute for Space-Earth Environmental Research (ISEE, International Joint Research Program, Nagoya University, Japan). VF, GV, IB thank the Royal Society, International Exchanges Scheme, collaborations with Instituto de Astrofisica de Canarias, Spain (IES/R2/212183), Institute for Astronomy, Astrophysics, Space Applications and Remote Sensing, National Observatory of Athens, Greece (IES/R1/221095), and Indian Institute of Astrophysics, India (IES/R1/211123) for the support provided.

References

Alharbi, A., Ballai, I., Fedun, V., & Verth, G. 2021, MNRAS, 501, 1940
Arber, T. D., Brady, C. S., & Shelyag, S. 2016, ApJ, 817, 94
Avrett, E. H., & Loeser, R. 2008, ApJS, 175, 229
Ballai, I. 2019, Front. Astron. Space Sci., 6, 39
Ballai, I., Forgács-Dajka, E., & McMurdo, M. 2024, Philos. Trans. Roy. Soc. London Ser. A, 382, 20230226
Ballester, J. L., Alexeev, I., Collados, M., et al. 2018, Space Sci. Rev., 214, 58
Brchnelova, M., Kuźma, B., Zhang, F., Lani, A., & Poedts, S. 2023, A&A, 678, A117
Carlsson, M., & Stein, R. F. 2002, ApJ, 572, 626
Cox, D. P., & Tucker, W. H. 1969, ApJ, 157, 1157
De Pontieu, B., McIntosh, S. W., Carlsson, M., et al. 2007, Science, 318, 1574
Khomenko, E., Collados, M., Díaz, A., & Vitas, N. 2014, Phys. Plasmas, 21, 092901
Kumar, M., Murawski, K., Kadowaki, L., Kuźma, B., & Kilpua, E. K. J. 2024, A&A, 681, A60
Leake, J. E., Lukin, V. S., Linton, M. G., & Meier, E. T. 2012, ApJ, 760, 109
Leenaarts, J., Carlsson, M., Hansteen, V., & Rutten, R. J. 2007, A&A, 473, 625
Leenaarts, J., Carlsson, M., Hansteen, V., & Gudiksen, B. V. 2011, A&A, 530, A124
Maneva, Y. G., Alvarez Laguna, A., Lani, A., & Poedts, S. 2017, ApJ, 836, 197
Martínez-Gómez, D. 2025, Phys. Plasmas, 32, 112101
Martínez-Gómez, D., Soler, R., & Terradas, J. 2017, ApJ, 837, 80
McMurdo, M., Ballai, I., Verth, G., Alharbi, A., & Fedun, V. 2023, ApJ, 958, 81
McMurdo, M., Ballai, I., Verth, G., & Fedun, V. 2025, ApJ, 988, 50
Moore, R. L., & Fung, P. C. W. 1972, Sol. Phys., 23, 78
Morton, R. J., Verth, G., Jess, D. B., et al. 2012, Nat. Commun., 3, 1315
Niedziela, R., Murawski, K., & Poedts, S. 2024, A&A, 691, A254
Okamoto, T. J., & De Pontieu, B. 2011, ApJ, 736, L24
Popescu Braileanu, B., Lukin, V. S., Khomenko, E., & de Vicente, Á. 2019, A&A, 630, A79
Smirnov, B. M. 2003, Physics of atoms and ions
Snow, B., & Hillier, A. 2021, A&A, 645, A81
Soler, R., Carbonell, M., & Ballester, J. L. 2013, ApJ, 209, 16
Vernazza, J. E., Avrett, E. H., & Loeser, R. 1981, ApJ, 45, 635
Voronov, G. S. 1997, Atomic Data Nucl. Data Tables, 65, 1
Yuan, D., Sadeghi, R., & Tavabi, E. 2026, Sol. Syst. Res., 60, 11
Zaqarashvili, T. V., Khodachenko, M. L., & Rucker, H. O. 2011, A&A, 529, A82

Appendix A: The elements of the matrix given by Eq. (20)

The coefficients $A_{i,j}$ were obtained by substituting the Fourier ansatz $\sim \exp[i(\omega t - k_x x - k_z z)]$ into the linearised equations, Eqs. (13)-(19), with $\partial/\partial t \rightarrow i\omega$ and $\nabla \rightarrow -i\mathbf{k}$, and then expressing the perturbations in terms of the dimensionless variables collected in Eq. (21).

For illustration, let us write the x-components of the ion and neutral momentum equations in the dimensionless form that is used in the dispersion relation; all the remaining equations can be rewritten in a similar fashion. Writing $k_x = k\sin\alpha$ and $k_z = k\cos\alpha$ (with α being the direction of propagation with respect to the direction of the ambient magnetic field), the components of the induction equation, Eq. (17), can be written as

$$b_x = -\frac{kB_0\cos\alpha}{\omega}v_{ix}, \quad b_z = \frac{kB_0\sin\alpha}{\omega}v_{ix}$$

The x-component of the ion momentum equation, Eq. (15), can be written as

$$\left(i\omega + \frac{\nu_{in}}{2} + n_{0i}K_R\right)v_{ix} - \left(\frac{\nu_{in}}{2} + n_{0n}K_I\right)v_{nx} -$$

$$-\frac{ik\sin\alpha}{m_i n_{0i}}p_i + \frac{ikB_0}{m_i n_{0i}\mu_0\omega}(b_x\cos\alpha - b_z\sin\alpha) = 0,$$

After introducing the expressions of the magnetic field perturbations, the above equation transforms into

$$\left(i\omega + \frac{\nu_{in}}{2} + n_{0i}K_R\right)v_{ix} - \left(\frac{\nu_{in}}{2} + n_{0n}K_I\right)v_{nx} -$$

$$-\frac{ik\sin\alpha}{m_i n_{0i}}p_i - \frac{ik^2v_A^2}{\omega}v_{ix} = 0,$$

Let us now divide the whole equation by the Alfvén frequency, kv_A and use the dimensionless quantities introduced earlier (see Eqs. 22 and 23). As a result, the x-component of the ion momentum equation becomes

$$(i\Omega + X/2 + \chi P)v_{ix} - (X/2 + \chi P)v_{nx} - \frac{i\sin\alpha p_i}{\rho_{0i}v_A} - \frac{i}{\Omega}v_{ix} = 0,$$

Next, we divided the whole equation by the Alfvén speed and introduced the dimensionless eigenvectors so that the above equation becomes

$$(i\Omega + X/2 + \chi P)u_{ix} - (X/2 + \chi P)u_{nx} - \frac{i\sin\alpha p_i}{\rho_{0i}v_A^2} - \frac{i}{\Omega}u_{ix} = 0.$$

Let us now concentrate on the pressure form term. The ion pressure perturbation can be written in dimensionless form in terms of the equilibrium ion pressure, so we write

$$\frac{i\sin\alpha p_i}{\rho_{0i}v_A^2} = \frac{i\sin\alpha p_{i0}}{\rho_i v_A^2}\tilde{p}_i = \frac{i\sin\alpha c_{Si}^2}{\gamma v_A^2}\tilde{p}_i = \frac{i\sin\alpha\beta}{2}\tilde{p}_i$$

As a result, the x-component of the ion momentum equation becomes

$$\left(i\Omega(1 - 1/\Omega^2) + X/2 + \chi P\right)u_{ix} - (X/2 + \chi P)u_{nx} - \frac{i\sin\alpha\beta}{2}\tilde{p}_i = 0.$$

These coefficients form the third row of the matrix A.

In a similar fashion, from Eq. (16) we can write for the x-component of the neutral momentum equation that

$$\left(i\omega + \frac{\nu_{in}}{2\chi} + n_{0i}K_I\right)v_{nx} - \left(\frac{\nu_{in}}{2\chi} + \frac{K_R n_{0i}}{\chi}\right)v_{ix} - \frac{ik\sin\alpha p_n}{m_i n_{0n}} = 0,$$

Again, the coefficients multiplying the perturbations can be written in dimensionless form by dividing the whole equation by the Alfvén frequency, kv_A, so

$$\left(i\Omega + \frac{X}{2\chi} + P\right)v_{nx} - \left(\frac{X}{2\chi} + P\right)v_{ix} - \frac{i\sin\alpha p_n}{m_i n_{0n}v_A} = 0.$$

Perturbations are written in dimensionless form as a result of the division of the whole equation by the Alfvén speed, so we have

$$\left(i\Omega + \frac{X}{2\chi} + P\right)u_{nx} - \left(\frac{X}{2\chi} + P\right)u_{ix} - \frac{i\sin\alpha p_n}{m_i n_{0n}v_A^2} = 0.$$

Let us treat the last term separately. We can write

$$\frac{i\sin\alpha p_{0n}}{\rho_{0n}v_A^2}\tilde{p}_n = \frac{i\sin\alpha c_{Sn}^2}{\gamma v_A^2}\tilde{p}_n = \frac{i\sin\alpha c_{Si}^2}{2\gamma v_A^2}\tilde{p}_n = \frac{i\sin\alpha\beta}{4}\tilde{p}_n,$$

where we used the identity that $c_{Si}^2 = 2c_{Sn}^2$. As a result, the x-component of the neutral momentum equation becomes

$$\left(i\Omega + \frac{X}{2\chi} + P\right)u_{nx} - \left(\frac{X}{2\chi} + P\right)u_{ix} - \frac{i\sin\alpha\beta}{4}\tilde{p}_n = 0.$$

The coefficients that appear in the above equation are given as the entries on the fifth row of the matrix A.

After Fourier analysing the linearised equations and expressing all perturbations in terms of the dimensionless variables collected in Eq. (21), the system can be written in the compact matrix form as $\sum_{j=1}^{8} A_{ij}Y_j = 0, \quad i = 1\ldots 8$. Rows 1 and 2 follow from the ion and neutral continuity equations, rows 3 and 4 from the x- and z-components of the ion momentum equation, rows 5 and 6 from the corresponding components of the neutral momentum equation, and rows 7 and 8 from the ion and neutral energy equations. The non-trivial solutions of this homogeneous system are obtained by setting $det(A) = 0$, which yields the dispersion relation analysed in the main text. The determinant A is given as

$$A = \begin{bmatrix} A_{1,1} & A_{1,2} & A_{1,3} & 0 & A_{1,5} & 0 & 0 & 0 \\ A_{2,1} & A_{2,2} & 0 & A_{2,4} & 0 & A_{2,6} & 0 & 0 \\ 0 & 0 & A_{3,3} & A_{3,4} & 0 & 0 & A_{3,7} & 0 \\ 0 & 0 & 0 & 0 & A_{4,5} & A_{4,6} & A_{4,7} & 0 \\ 0 & 0 & A_{5,3} & A_{5,4} & 0 & 0 & 0 & A_{5,8} \\ 0 & 0 & 0 & 0 & A_{6,5} & A_{6,6} & 0 & A_{6,8} \\ A_{7,1} & A_{7,2} & A_{7,3} & 0 & A_{7,5} & 0 & A_{7,7} & A_{7,8} \\ A_{8,1} & A_{8,2} & 0 & A_{8,4} & 0 & A_{8,6} & A_{8,7} & A_{8,8} \end{bmatrix}$$

Each element $A_{i,j}$ is presented in the dimensionless form and is defined as follows:

$A_{1,1} = i\Omega + P\chi, \quad A_{1,2} = -P\chi, \quad A_{1,3} = -i\sin\alpha, \quad A_{1,5} = -i\cos\alpha$
$A_{2,1} = -P, \quad A_{2,2} = i\Omega + P, \quad A_{2,4} = -i\sin\alpha, \quad A_{2,6} = -i\cos\alpha$
$A_{3,3} = i\Omega(1 - 1/\Omega^2) + X/2 + P\chi, \quad A_{3,4} = -(X/2 + P\chi),$
$A_{3,7} = -i\sin\alpha\beta/2,$
$A_{4,5} = i\Omega + X/2 + P\chi, \quad A_{4,6} = -(X/2 + P\chi), \quad A_{4,7} = -i\cos\alpha\beta/2,$
$A_{5,3} = -(X/2\chi + P), \quad A_{5,4} = i\Omega + X/2\chi + P, \quad A_{5,8} = -i\sin\alpha\beta/4,$
$A_{6,5} = -(X/2\chi + P), \quad A_{6,6} = i\Omega + X/2\chi + P, \quad A_{6,8} = -i\cos\alpha\beta/4,$
$A_{7,1} = -(3X/2 + \hat{\Phi}P\chi\gamma), \quad A_{7,2} = 3X/2 + \hat{\Phi}P\gamma\chi,$
$A_{7,3} = -i\sin\alpha\gamma/(\gamma - 1),$
$A_{7,5} = -i\cos\alpha\gamma/(\gamma - 1), \quad A_{7,7} = i\Omega/(\gamma - 1) + 3X/2 + 3\chi P/2,$
$A_{7,8} = -3/4(X + P\chi)$
$A_{8,1} = 3X/\chi, \quad A_{8,2} = -3X/\chi, \quad A_{8,4} = -i\sin\alpha\gamma/(\gamma - 1),$
$A_{8,6} = -i\cos\alpha\gamma/(\gamma - 1), \quad A_{8,7} = -3(X/\chi + P),$
$A_{8,8} = i\Omega/(\gamma - 1) + 3X/2\chi + 3P/2.$